J. Membrane Biol. 211, 173–184 (2006)
DOI: 10.1007/s00232-006-0036-z

The Journal of
Membrane
Biology

A Kir2.3-like K^+ Conductance in Mouse Cortical Collecting Duct Principal Cells

I.D. Millar[1], H.C. Taylor[1], G.J. Cooper[1], J.D. Kibble[2], L. Robson[1]
[1]Department of Biomedical Science, University of Sheffield, Sheffield S10 2TN, United Kingdom
[2]Medical Physiology, St. George's University, PoB 7, Grenada

Received: 1 June 2006/Revised: 11 July 2006

Abstract. K^+ channels play an important role in renal collecting duct cell function. The current study examined barium (Ba^{2+})-sensitive whole-cell K^+ currents (*I*KBa) in mouse isolated collecting duct principal cells. *I*KBa demonstrated strong inward rectification and was inhibited by Ba^{2+} in a dose- and voltage-dependent fashion, with the K_d decreasing with hyperpolarization. The electrical distance of block by Ba^{2+} was around 8.5%. As expected for voltage-dependent inhibition, the association constant increased with hyperpolarization, suggesting that the rate of Ba^{2+} entry was increased at negative potentials. The dissociation constant also increased with hyperpolarization, consistent with the movement of Ba^{2+} ions into the intracellular compartment at negative potentials. These properties are not consistent with ROMK but are consistent with the properties of Kir2.3. Kir2.3 is thought to be the dominant basolateral K^+ channel in principal cells. This study provides functional evidence for the expression of Kir2.3 in mouse cortical collecting ducts and confirms the expression of Kir2.3 in this segment of the renal tubule using reverse-transcriptase polymerase chain reaction. The conductance described here is the first report of a macroscopic K^+ conductance in mouse principal cells that shares the biophysical profile of Kir2.3. The properties and dominant nature of the conductance suggest that it plays an important role in K^+ handling in the principal cells of the cortical collecting duct.

Key words: Potassium ion channel — Patch clamp — Renal physiology

Correspondence to: L. Robson; email: l.robson@sheffield.ac.uk

Introduction

K^+ channels play a vital role in renal epithelial cells, participating in generation of the resting membrane potential, maintenance of transport function, regulation of cell volume as well as K^+ secretion and K^+ homeostasis. Patch-clamp studies have identified a wide variety of K^+ channel types located on both the apical and basolateral membranes of the cells of the proximal tubule, thick ascending limb and the collecting duct. In the collecting duct, K^+ channels are particularly important in principal cell function and play a pivotal role in renal K^+ secretion and K^+ homeostasis. Transport by the principal cells is driven by a basolateral Na^+/K^+-adenosine triphosphatase (ATPase), which maintains a low intracellular Na^+ concentration. This low Na^+ concentration provides the driving force for Na^+ uptake across the apical membrane via the epithelial Na^+ channel (ENaC). Apical Na^+ uptake then drives the secretion of K^+ across the apical membrane via a small-conductance apical K^+ channel. On the basolateral membrane, K^+ channels recycle K^+ that enters via the Na^+/K^+-ATPase, and they may also play role in K^+ secretion. Patch-clamp studies have identified two individual basolateral K^+ channels in principal cells of the rat. A low-conductance, barium (Ba^{2+})-sensitive, inwardly rectifying channel is thought to provide the main basolateral K^+ conductance (Lu & Wang, 1998), while there is also a Ba^{2+}-sensitive, hyperpolarization-activated intermediate conductance channel (Wang, 1995). Macroscopically, the basolateral K^+ conductance in rat principal cells was recently shown to have weakly inwardly rectifying properties (Gray et al., 2005).

At the molecular level, there are three distinct families of K^+ channels: the voltage-dependent K^+ channel family (Kv), the inwardly rectifying family (Kir) and the two-pore domain family. Kv channel proteins have six transmembrane spanning domains

and one region that codes for the channel pore (Doyle et al., 1998). Kir channels also have one pore region but only two transmembrane spanning domains (Kubo et al., 1993). In contrast, the two-pore family of channels has four transmembrane spanning domains and two pore regions (Lesage et al., 1996). At the present time, few renal K^+ channels have been identified at the molecular level. One of these channels, ROMK (Kir1.1), is an inwardly rectifying, ATP-sensitive K^+ channel that forms the small-conductance K^+ channel observed on the apical membrane of the principal cells of the collecting duct (Ho et al., 1993; Xu et al., 1997). Another inwardly rectifying K^+ channel identified at the molecular level is CCD-IRK_3 (Kir2.3) (Welling, 1997). This channel demonstrates a strong inwardly rectifying profile. It has been suggested that this channel forms the dominant basolateral K^+ conductance. Kir2.3 was initially identified from a collecting duct cell line (M1), and mRNA for Kir2.3 is found in mouse kidney (Welling, 1997). In addition, targeting studies have demonstrated that Kir2.3 localizes to the basolateral membrane in MDCK cells (Le Maout et al., 1997). However, a comparison of the properties of the macroscopic basolateral K^+ conductance with Kir2.3 in mouse principal cells has not been conducted to date. Certainly, the macroscopic basolateral K^+ conductance in rat principal cells has a weakly inwardly rectifying profile (Gray et al., 2005), inconsistent with a role for Kir2.3 in basolateral K^+ conductance. The aim of the present study was to examine the properties of the K^+ conductance in mouse collecting duct principal cells and relate them to Kir2.3.

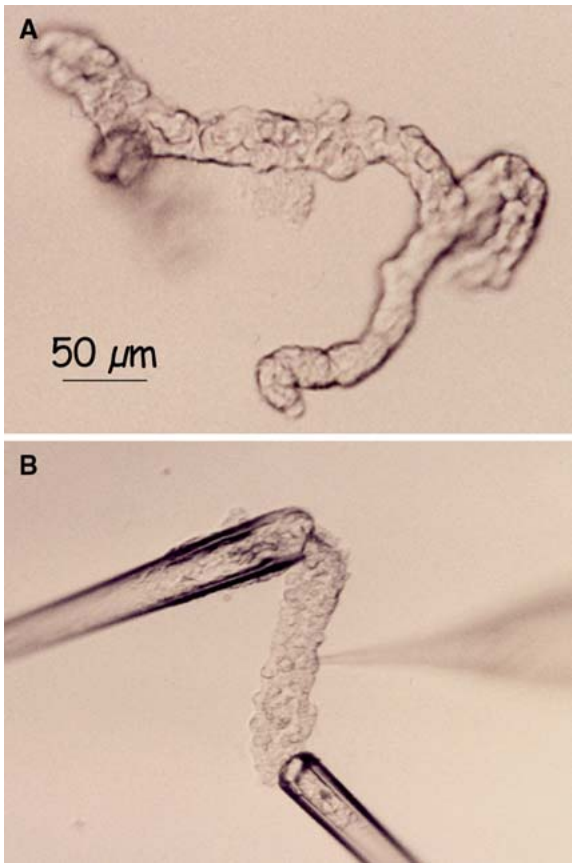

Fig. 1. (*A*) Cortical collecting duct demonstrating a typical bifurcation. (*B*) Cortical collecting duct held in position with two glass pipettes. The patch pipette can be seen on the right. In both images, note the presence of flat cells, which show a typical principal cell electrophysiological profile, and rounded cells, which demonstrate a typical intercalated cell electrophysiological profile.

Methods

Animal Model

Collecting ducts were isolated from C57/B6 mice of both sexes and over 6 weeks of age.

Tubule Isolation

Single collecting ducts were isolated using a protocol modified from that of Schafer et al. (1998). Adult mice were killed humanely, according to UK legislation, by cervical dislocation. The kidneys were rapidly removed and placed in ice-cold modified Eagle's medium (MEM). After removing the capsule, a single layer of thin (< 0.5 mm), tangential slices was taken from the entire cortex. These cortical slices were then torn into pieces and placed in a 25-ml conical flask containing 2 ml of MEM plus type II collagenase (0.5 mg/ml), protease E (0.1 mg/ml), soybean trypsin/chymotrypsin inhibitor (50 μg/ml) and glycine (5 mM). The flask was gently agitated for 10 s and then incubated at 37°C without further agitation. During incubation, tubules were slowly liberated into the digestion medium; and at 10-min intervals, the digestion medium and tubules were decanted from the flask into a test tube. The incubation medium in the flask was replaced and the flask placed back in the water bath. Decanted medium was placed on ice, and tubules were allowed to settle to the bottom of the tube (approximately 4 min). After this time, the supernatant was gently removed and replaced with 2 ml ice-cold MEM plus 1% bovine serum albumin. The tubules were stored on ice until required. Collecting ducts were identified by their bifurcations (Fig. 1A) (Schafer et al., 1998).

Patch Experiments

Collecting ducts were placed in a Perspex bath on the stage of an inverted microscope (IX70; Olympus, Tokyo, Japan) and held in place using two holding pipettes. Standard patch-clamp experiments were employed to investigate whole-cell currents (Hamill et al., 1981). Voltage protocols were driven from an IBM-compatible computer equipped with a Digidata Interface (Axon Instruments, Burlingame, CA) using the pClamp software Clampex (Axon Instruments). Recordings were made using a List EPC-7 amplifier (List Electronic, Darmstadt-Eberstadt, Germany). To reduce stray capacitance, patch pipettes were coated with Sylgard (Dow Corning, Midland, MI). Reversal potentials (V_{rev}) in voltage-clamp experiments were determined using polynomial regression. Tubules were superfused using a small-volume, fast-exchange perfusion system (Automate; Digitimer, Welwyn Gorden City UK).

Whole-cell clamp was obtained via the basolateral aspect of the tubules. Principal and intercalated cells were identified

both morphologically and electrophysiologically (see Fig. 1 and Results). Currents were saved directly onto the hard disk of the computer following low-pass filtering at 5 kHz. In current-clamp experiments, cell current was clamped to zero and reversal potentials were recorded using pClamp 8. In voltage-clamp experiments, cell potential was clamped at a holding potential of −40 mV and then stepped to between +100 and −100 mV, in −20-mV steps. Average currents at each potential were derived using Microsoft Excel 2000. Instantaneous currents were recorded 10 ms from the start of a potential step, while steady-state currents were recorded at the end of the potential step. In voltage-clamp experiments, cell area was calculated from the capacity transients seen in response to a 20-mV potential step, with membrane capacitance assumed to be 1 $\mu F/cm^2$. The mean capacitance of principal cells was 11.0 ± 0.63 pF (n = 34).

Current-Clamp Experiments

Whole-cell clamp was obtained with Na^+ Ringer in the bath, which contained (in mM) 135 NaCl, 5 KCl, 2 $CaCl_2$, 1 $MgCl_2$, 10 mannitol and 10 4-(2-hydroxyethyl)-1-piperazineethanesulfonic acid (HEPES, titrated to pH 7.4 with NaOH). The pipette contained (in mM) 145 KCl, 0.5 ethyleneglycoltetraacetic acid (EGTA), 10 mannitol and 10 HEPES (titrated to pH 7.4 with KOH). On achieving the whole-cell configuration, cell current was clamped to zero and V_{rev} measured with high-Na^+ Ringer and then either (1) high KCl (in mM: 100 KCl, 40 NaCl, 2 $CaCl_2$, 1 $MgCl_2$, 10 mannitol and 10 HEPES), to determine K^+ selectivity; (2) 5 mM Ba^{2+} (removal of 10 mM mannitol from Na^+ Ringer), to examine blocker sensitivity; or (3) Na^+ gluconate (in mM: 35 NaCl, 100 Na^+ gluconate, 2 $CaCl_2$, 1 $MgCl_2$, 10 mannitol and 10 HEPES), to determine Cl^- selectivity.

Voltage-Clamp Experiments

Whole-cell patch-clamp experiments under voltage-clamp conditions were then utilized to examine K^+ currents in principal cells. Cells were clamped between +100 and −100 mV in −20-mV steps. Whole-cell clamp was obtained with Na^+ Ringer in the bath, which contained (in mM) 135 NaCl, 5 KCl, 2 $CaCl_2$, 1 $MgCl_2$, 10 mannitol and 10 HEPES (titrated to pH 7.4 with NaOH). The pipette contained (in mM) 145 KCl, 0.5 EGTA, 10 mannitol and 10 HEPES (titrated to pH 7.4 with KOH). This gave a Nernst potential for K^+ of −85 mV. On achieving the whole-cell configuration, cellular currents were initially recorded in Na^+ Ringer followed by high K^+ (135 mM NaCl replaced with 135 mM KCl). The V_{rev} under each condition was measured and the relative K^+:Na^+ selectivity of the cells was calculated using the Goldman equation. The Ba^{2+} sensitivity of currents was determined from the effect of addition of 5 mM Ba^{2+} to the bath (osmolality maintained by mannitol removal) in either Na^+ Ringer or high-K^+ Ringer. The dose response to Ba^{2+} was determined in a modified high-K^+ Ringer, which contained 140 mM KCl, 2 mM $CaCl_2$, 1 mM $MgCl_2$, 20 mM mannitol and 10 mM HEPES. The concentration of Ba^{2+} was altered between 1 μM and 10 mM (osmolality maintained by removal of mannitol).

Reverse-Transcriptase Polymerase Chain Reaction Determination of mRNA Expression

To examine the expression of Kir2.1, Kir2.2 and Kir2.3 in mouse collecting ducts and to confirm the identity of tubule segments used in electrophysiological experiments, reverse-transcriptase polymerase chain reaction (RT-PCR) was carried out on RNA obtained either from cortical collecting ducts sorted from the tubule preparation or from unsorted tubules taken from whole cortex. Samples were screened for the following gene markers: ENaC (Genebank accession NM011324), γ-glutamyltransferase 1 (γGT, NM008116), uromodulin (NM009470), Kir2.1 (NM008425), Kir2.2 (NM008426) and Kir2.3 (NM008427).

Total RNA was extracted from whole-cortex tubules or cortical collecting duct tubules using the NucleoSpin RNA II kit (Machergy-Nagel, Düren, Germany). First-strand cDNA synthesis was performed using Superscript II (Invitrogen, Paisley, UK) in combination with an oligoDT primer as directed by the manufacturer's instructions. For the whole-cortex samples, approximately 2.5 ng of total RNA was used in the RT reaction and, in the case of isolated collecting ducts, experiments started with 0.05 ng of RNA. In each case, a control reaction was performed in which the Superscript enzyme was omitted. Amplification of cDNA by PCR was performed in a thermocycler (Techne, Stone, UK) using the enzyme *Taq* DNA polymerase (Eppendorf, Cambridge, UK). Oligonucleotide primers were designed to amplify 400–500 bp fragments of ENaC, γGT, uromodulin, Kir2.1, Kir2.2 and Kir2.3 (the details of individual primers and expected product sizes are given in Table 1). Samples were subjected to either 40 (whole cortex) or 50 (isolated collected ducts) cycles comprised of denaturation for 30 s at 94°C, annealing (see Table 1 for temperature details) for 30 s and extension for 45 s at 72°C. A final extension phase of 72°C for 10 min was included for all samples. PCR products were separated by electrophoresis on a 2% agarose gel and visualized by ethidium bromide staining under ultraviolet (302 nm) light. To verify the identity of the PCR products, we carried out restriction endonuclease digestion. Details of the enzymes used and the predicted sizes of the product bands are given in Table 1. RT-PCR was repeated at least three times on RNA from three separate extractions.

Solutions

All chemicals were obtained from Sigma (St. Louis, MO). Osmolality of the experimental solutions was checked using a Roebling (Berlin Germany) osmometer and adjusted to 300 ± 1 mOsm · kg^{-1} H_2O using mannitol or water as appropriate.

Statistics

Results are presented as mean ± standard error of the mean (SEM). Effects of experimental interventions were assessed by paired Student's t-test, and significance was assumed at the 5% level.

Results

Current-Clamp Experiments

In principal cells with high bath Na^+, the initial V_{rev} on achieving the whole-cell configuration was −59.4 ± 2.14 mV (n = 15). On addition of high K^+ to the bath, the V_{rev} shifted in a depolarizing direction, followed by recovery on washout in high Na^+ (Table 2). Addition of Na^+ gluconate to the bath gave a hyperpolarizing shift in V_{rev} at steady state, while addition of 5 mM Ba^{2+} to the bath depolarized V_{rev} in a reversible manner by +33.3 ± 3.79 mV (n = 11) (Table 2). In contrast, in intercalated cells, the initial V_{rev} in high Na^+ was −3.49 ± 2.04 (n = 13). Addition of high K^+ to the bathing

Table 1. Summary of the composition of primers used in PCRs on isolated collecting duct and whole kidney samples

Primer	Sequence (5′–3′)	Annealing temperature (°C)	Predicted product size (bp)	Restriction endonuclease used	Predicted cut sizes (bp)
ENaC	Sense 5′-GCTCCTGGGGCTACTGCTACTA-3′ Antisense 5′-CGGCTCCGGAACCTGTG-3′	55	421	*Hinf*I	160, 260
γ-GT	Sense 5′-GCGCCAAGGCCTTCTACAAT-3′ Antisense 5′-GCGGCTGGGTGGGTGGTTTCAT-3′	55	430	*Sac*I	370, 60
THF	Sense 5′-CTGGATGTCCATAGTGACTC-3′ Antisense 5′-TGTGGCATAGCAGTTGGTCA-3′	55	400	*Nco*I	200, 200
Kir2.1	Sense 5′-CATGCGTGTCGGAGGTCAAC-3’ Antisense 5′-ATGCGGTCAATTCCACTATCAAAA-3′	57	421	*Dra*III	116, 305
Kir2.2	Sense 5′-TCAATGCCGGAGTTCGTATCT-3′ Antisense 5′-GCTGCTTGCTTTCACCCACCTCT-3’	55	477	*Bgl*II	182, 295
Kir2.3	Sense 5′-TGGCGGTCATTGCGGTGGTTGT-3′ Antisense 5′-GGAGCTGCGGGCCTGAGTGGTC-3′	62	476	*Dra*III	200, 276

Column 3 gives details of the annealing temperatures used for each primer set. Column 4 provides the size of the predicted PCR product. Column 5 provides information regarding a suitable restriction endonuclease used to cleave the PCR product, with the size of the digested bands given in the final column.

Table 2. Current-clamp measurements from principal (PC) and intercalated (IC) cells

	V_{rev} (mV)					
	NaCl (n = 15 PCs, 13 ICs)	KCl	NaCl	NaCl (n = 5 PCs, 10 Ics)	NaGluc	NaCl
PC	−59.4 ± 2.14	−9.40 ± 0.54*	−53.8 ± 2.68	−60.4 ± 2.73	−67.5 ± 4.66**	−63.9 ± 4.07
IC	−3.49 ± 2.04	−4.22 ± 1.53	−3.39 ± 2.00	−2.30 ± 2.08	9.33 ± 4.67*	−2.30 ± 2.47
	NaCl (n = 11 PCs, 13 ICs)	Ba^{2+}	NaCl			
PC	−56.1 ± 3.50	−22.8 ± 4.24*	−47.7 ± 5.17			
IC	−3.99 ± 2.23	−3.81 ± 2.14	−4.43 ± 2.57			

The effect of experimental interventions was examined using Student's paired t-test.
Significant differences from NaCl, *$P < 0.01$ and **$P = 0.02$.

solution superfusing intercalated patches did not give a significant shift in V_{rev} (Table 2). However, superfusion of intercalated cells with Na^+ gluconate shifted the V_{rev} in a positive direction by +11.6 ± 3.09 mV (n = 10) (Table 2). Like high K^+, Ba^{2+} was without effect (Table 2).

Voltage-Clamp Experiments

Total Current Profile: NaCl Ringer

The total whole-cell currents in principal cells showed a characteristic profile. Figure 2A shows a typical whole-cell current recording, and Figure 2B shows the mean currents recorded from 13 cells. The initial current recorded on stepping the potential demonstrated weak inward rectification and had a V_{rev} of −38.3 ± 5.04 mV (n = 13). However, at steady state the currents demonstrated strong inward rectification and had a V_{rev} of −68.3 ± 5.04 mV (n = 13). The strong inward rectification was a consequence of inactivation of the total conductance over the potential range +100 to −20 mV (Fig. 2C) ($P \leq 0.01$).

Effect of KCl Ringer on Total Current

To examine K^+:Na^+ selectivity, the bath solution was exchanged for one containing a total of 140 mM KCl (135 mM NaCl replaced by 135 mM KCl) (Fig. 3). Addition of K^+ to the bath shifted the V_{rev} of initial currents by +52.9 ± 2.47 mV (n = 14, $P < 0.001$), corresponding to a K^+:Na^+ selectivity ratio of 15.9 ± 3.81. Similarly, K^+ shifted the V_{rev} of steady-state currents from −69.7 ± 1.35 to 0.28 ± 0.29 mV (n = 14, $P < 0.001$), a shift of +70.0 ± 1.27 mV corresponding to a K^+:Na^+ selectivity ratio of 40.1 ± 4.91. The shift in steady-state currents was significantly greater than the shift observed in the initial currents ($P < 0.001$).

Both the initial and steady-state currents in KCl demonstrated inward rectification (Fig. 3B). The initial conductance at +100 mV was 0.53 ± 0.05 times the conductance at −100 mV, 1,840 ± 262 *vs.* 3,705 ± 612 μS/cm^2 (n = 14, $P < 0.001$). However, rectification of steady-state currents was again more marked than that of initial currents. The steady-state conductance at +100 mV was 0.22 ± 0.03 times

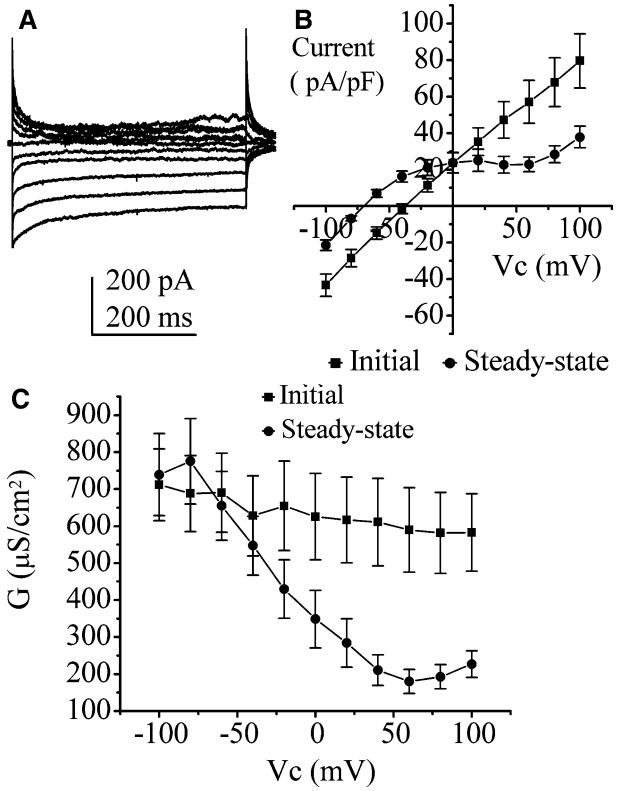

Fig. 2. (*A*) Typical whole-cell currents recorded from a single cell with NaCl in the bath. (*B*) Mean initial (■) and steady-state (●) total currents recorded with NaCl in the bath. (*C*) Mean initial (■) and steady-state (●) conductances. (*B, C*) $n = 13$.

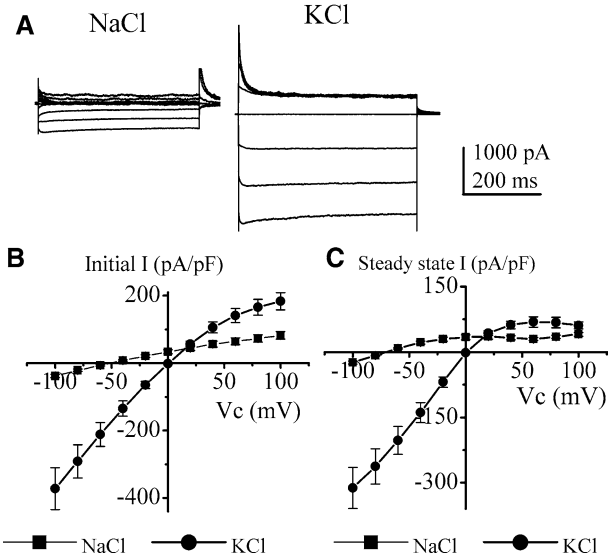

Fig. 3. (*A*) Typical whole-cell currents recorded from a single cell with bath NaCl (*left*) and KCl (*right*). (*B*) Mean initial currents recorded with extracellular NaCl (■) and KCl (●). (*C*) Mean steady-state currents recorded with extracellular NaCl (■) and KCl (●). (*B, C*) $n = 14$.

the conductance at −100 mV, 614 ± 82 *vs.* 3,102 ± 464 μS/cm^2 ($n = 14$, $P < 0.001$).

Effect of Ba^{2+}

It was clear from examination of the total currents that whole-cell currents were K^+-selective and that at steady state the currents had a greater K^+ selectivity than initial currents. This suggested that more than one conductance type was present in the cells and that the initial currents were partly comprised of a conductance that was not as K^+-selective (Millar et al., 2006). Therefore, to dissect out the Ba^{2+}-sensitive, K^+-selective current, the effect of Ba^{2+} was examined.

In NaCl Ringer, addition of 5 mM Ba^{2+} to the bath decreased both initial and steady-state currents (Fig. 4A) ($P < 0.05$). The V_{rev} of total initial currents depolarized from −40.5 ± 6.54 to −14.1 ± 3.68 mV ($n = 10$, $P < 0.001$), while the V_{rev} of the total steady-state currents depolarized from −67.9 ± 3.84 to −22.0 ± 3.18 mV ($n = 10$, $P < 0.001$). Subtraction of the currents recorded in the presence of Ba^{2+} from control currents gave the Ba^{2+}-sensitive currents. Steady-state Ba^{2+}-sensitive currents had an inwardly rectifying profile and showed inactivation at positive potentials (Fig. 5A). There was no significant difference between the V_{rev} of the initial and steady-state Ba^{2+}-sensitive currents, −68.5 ± 3.92 *vs.* −76.3 ± 2.70 mV ($n = 10$), respectively. The steady-state conductance was modeled to the Boltzman equation (equation 1) (Fig. 5B).

$$G = \frac{G\,max}{1 + \exp\left[\frac{w\,F(Vm - Vo)}{RT}\right]} \quad (1)$$

where G_{max} is the maximum conductance (μS/cm^2), w is the gating charge, V_m is the clamp potential (mV), V_o is the potential at which the conductance is half-maximal (mV) and RT and F have their standard values. For steady state currents in NaCl, V_o was −19.6 ± 9.01 mV, w was 1.34 ± 0.17 and G_{max} was 671.7 ± 113.7 μS/cm^2 ($n = 10$).

In KCl Ringer, addition of 5 mM Ba^{2+} to the bath also decreased both initial and steady-state inward currents (Fig. 4C) ($n = 7$, $P < 0.05$). The steady-state Ba^{2+}-sensitive currents had inwardly rectifying profiles (Fig. 5C), with apparent inactivation of the current observed at potentials more positive than +20 mV ($P < 0.05$). The steady-state conductance (GKBa) was modeled to the Boltzman equation (equation 1) (Fig. 5C). For steady-state currents in KCl V_o was 15.0 ± 3.17 mV, w was 1.29 ± 0.16 and G_{max} was 3,048.2 ± 615.5 μS/cm^2 ($n = 7$).

In unpaired cells, the shift in V_{rev} of the initial Ba^{2+}-sensitive currents when extracellular Na^+ was substituted with K^+ was −68.4 mV (−68.5 ± 3.92

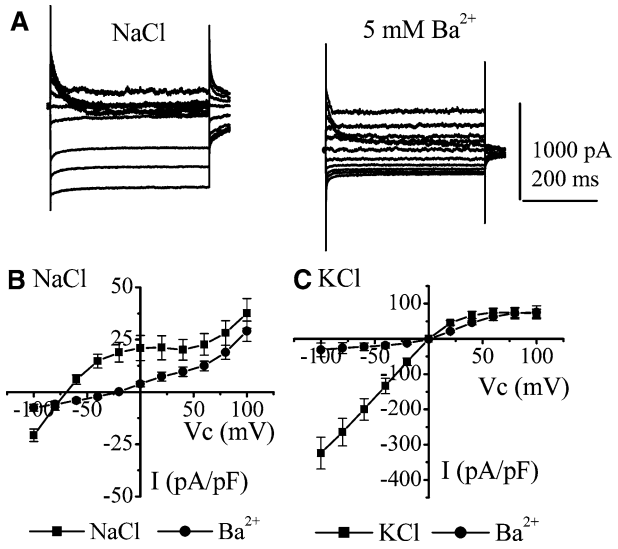

Fig. 4. (*A*) Typical whole-cell currents recorded from a single cell in the absence (*left*) and presence (*right*) of 5 mM Ba^{2+}. (*B*) Mean effect of Ba^{2+} on steady-state currents with NaCl in the bath (n = 10). (*C*) Mean effect of Ba^{2+} on steady-state currents with KCl in the bath (n = 7).

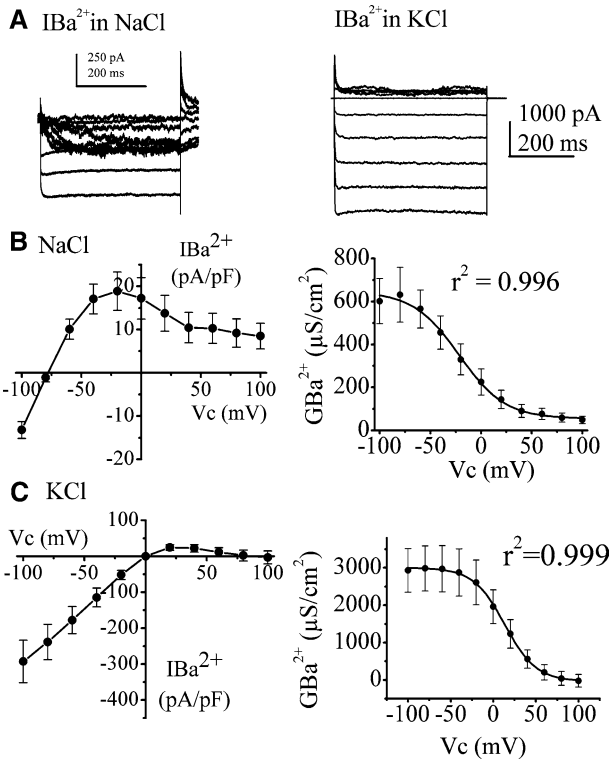

Fig. 5. (*A*) Typical Ba^{2+}-sensitive currents recorded with either Na^+ (*left*) or K^+ (*right*) as the dominant extracellular cation. (*B*) With Na^+ in the bath, mean Ba^{2+}-sensitive currents (*left*) and Ba^{2+}-sensitive conductance (*right*) (n = 10). (*C*) With K^+ in the bath, mean Ba^{2+}-sensitive currents (*left*) and Ba^{2+}-sensitive conductance (*right*) (n = 7). Lines through conductance data are the best fit to the Boltzman equation (equation 1), with the degree of fit given for each graph.

mV, n = 10, to −0.13 ± 0.54 mV, n = 7). This corresponded to an Na^+:K^+ selectivity ratio of 0.03. The shift in V_{rev} of the steady-state Ba^{2+}-sensitive currents when extracellular Na^+ was substituted with K^+ was −75.1 mV (−76.3 ± 2.70 mV, n = 10, to −1.23 ± 1.11 mV, n = 7). This corresponded to an Na^+:K^+ selectivity ratio of 0.02.

Dose Response to Ba^{2+}

Ba^{2+} blocked currents in a dose-dependent manner (Fig. 6). Inward currents were maximally inhibited with 5 mM Ba^{2+} (P > 0.05 compared to 10 mM). Maximal inhibition of outward currents with 5 mM Ba^{2+} was observed at all potentials up to +20 mV. Addition of 10 mM Ba^{2+} between +40 and +100 mV gave a small but significant increase in block (P < 0.05).

Inhibition by Ba^{2+} was also voltage-dependent. This is clearly seen in Figure 6A, which shows a typical steady-state current voltage curve obtained from a single cell. At 100 μM and 1 mM Ba^{2+}, an increase in relative inhibition was observed at more negative potentials. The Hill equation (equation 2) was used to calculate the half-maximal inhibitory concentrations (K_d) over the potential range −20 to −100 mV.

$$\frac{\mathrm{IKBa}}{\mathrm{IKmax}} = \frac{1}{1 + \left[\frac{[\mathrm{Ba}^{2+}]}{\mathrm{K_d}}\right]^n} \qquad (2)$$

where IKBa is the Ba^{2+}-sensitive current at a given Ba^{2+} concentration, $I\mathrm{K}_{max}$ is the maximum Ba^{2+}-sensitive current (obtained from 10 mM Ba^{2+} data), K_d is the concentration giving half-maximal inhibition (μM) and n is the Hill coefficient. Figure 7A. shows data obtained from a single patch, while Fig. 7B. shows the mean K_d values from six cells. Consistent with voltage-dependent block, the more negative the potential, the smaller the K_d. The mean Hill coefficients for the data were 0.68 ± 0.10, 0.64 ± 0.12, 0.61 ± 0.10, 0.62 ± 0.08 and 0.66 ± 0.08 at −20, −40, −60, −80 and −100 mV, respectively, suggesting that one Ba^{2+} molecule was required for inhibition. The line through the data points in Figure 7B is the best fit to the Woodhull equation (equation 3), with Y data represented by the K_d values. For these data, δ was 8.5%, $K_d(0)$ was 335 μM and r^2 was 0.997.

$$\mathrm{Y} = \mathrm{Y}(0) \times \exp\left[\frac{z\delta \mathrm{F}}{\mathrm{RT}}\mathrm{V}\right] \qquad (3)$$

where Y_0 represents the value of Y at 0 mV, z is the valency of Ba^{2+} (+2), δ is the electrical distance between the Ba^{2+} blocking site and the outer pore of the channel and RT and F have their usual values.

To examine further the kinetics of inhibition by Ba^{2+}, the time constants of block observed with

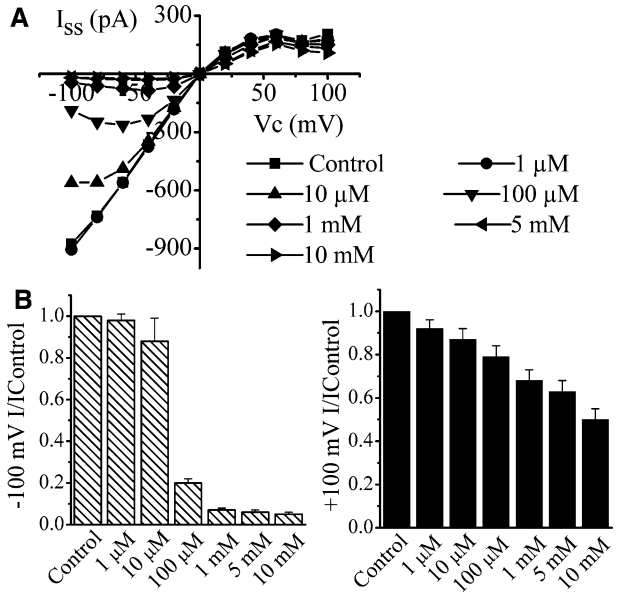

Fig. 6. (*A*) Steady-state Ba^{2+}-sensitive currents (I_{SS}) in a typical cell for Ba^{2+} concentrations varying between 1 μM and 10 mM. (*B*) Mean Ba^{2+}-sensitive currents at −100 (*left*) and +100 (*right*) mV expressed as a fraction of control for Ba^{2+} concentrations between 0 and 10 mM ($n = 6$).

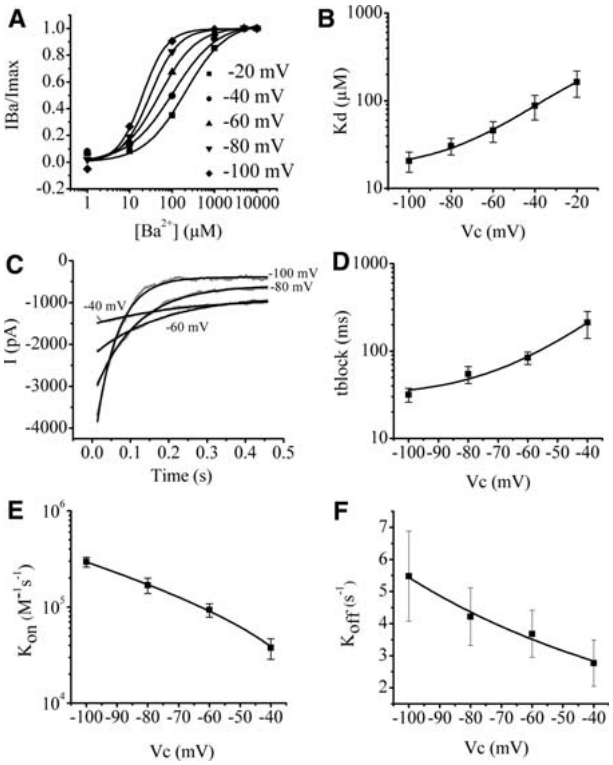

Fig. 7. (*A*) Dose response to Ba^{2+} in a typical cell over the potential range −100 to −20 mV. *Lines* through data points are best fit to the Hill equation (equation 2). (*B*) Mean K_d values calculated from the dose response to Ba^{2+} at different potentials. (*C*) Typical traces (*gray*) obtained from a single cell in the presence of 100 μM Ba^{2+} (leak subtraction performed with the 5 mM Ba^{2+} trace). *Black lines* indicate the best fit to a single exponential. (*D*) Mean time constant of Ba^{2+} block against potential. (*E*) Mean association constant *vs.* potential. (*F*) Mean dissociation constant *vs.* potential. (*B, D-F*) *Lines* through data are the best fit to the Woodhull equation (equation 3) ($n = 6$).

100 μM Ba^{2+} (τ) were calculated using single exponential fits to the traces obtained over the range −100 to −40 mV. The currents recorded with 5 mM Ba^{2+} (maximal inhibitory concentration over this potential range) were subtracted from all traces for apparent leak current correction. Figure 7C shows exponential fits to currents recorded from a single cell, while Figure 7D shows the mean τ for six cells. The line in Figure 7D is the best fit to the Woodhull equation (equation 3), with the Y data represented by τ. The electrical distance (δ) was 9.2%, τ_0 was 1,160 ms and r^2 was 0.985. This value for δ was similar to that calculated using the dissociation constants (8.5%). The association (K_{on}) and dissociation (K_{off}) rate constants for Ba^{2+} binding to the inhibitory site were then calculated according to equations 4 and 5, respectively (Holmgren, Smith & Yellen, 1997; Shieh, Chang & Arreola, 1998).

$$K_{on} = \frac{1 - f}{\tau[Ba^{2+}]} \tag{4}$$

$$K_{off} = \frac{f}{\tau} \tag{5}$$

where $f = I_{steady\ state}/I_{control}$ and τ is the time constant of block. Figure 7E shows the mean K_{on}, while Figure 7F shows the mean K_{off}. The lines through both sets of data are the best fit to the Woodhull equation (equation 3), with Y represented by either K_{on} or K_{off}. Both K_{on} and K_{off} were voltage-dependent. As expected for the voltage-dependent block, K_{on} increased with more negative potentials. The Boltzman fit to the data gave the electrical distance (δ) as 3.7%, which was again similar to values obtained from the K_d and τ. The association constant at 0 mV was 13.3×10^3 $M^{-1}s^{-1}$ and r^2 was 0.979. Interestingly, K_{off} also increased with more negative potentials. From the Boltzman fit, δ was 10.2%, K_{off} at 0 mV was 2.15 s^{-1} and r^2 was 0.975.

RT-PCR Determination of mRNA Expression

Data from the RT-PCR experiments are given in Figure 8. In whole-cortex samples, mRNA for ENaC, Kir2.1, Kir2.2, Kir2.3, γGT and uromodulin were detected. However, in RNA samples taken from collecting ducts that were morphologically identified as described previously, only ENaC (a collecting duct marker) and Kir2.3 were detected. In contrast, mRNA for γGT and uromodulin, markers for proximal tubule and thick ascending limb, respec-

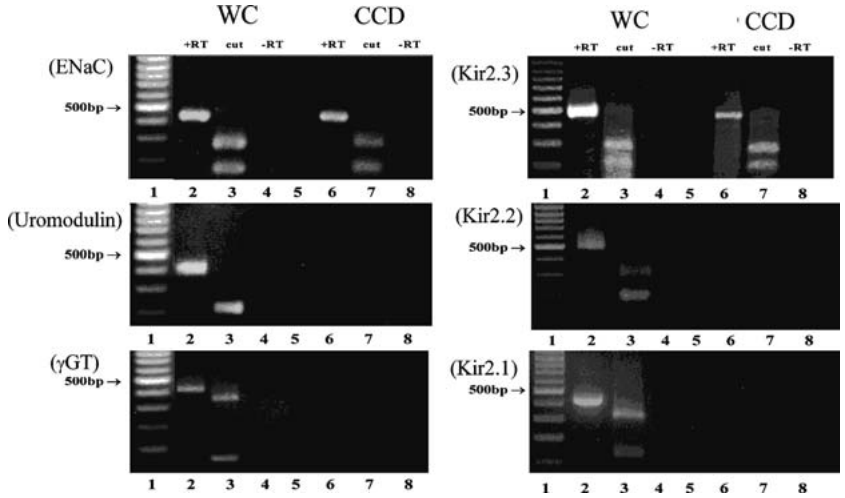

Fig. 8. Expression of mRNA in mouse whole cortex (*WC*) and cortical collecting ducts (*CCD*). Representative agarose gels showing products amplified from mouse kidney and mouse collecting ducts by PCR. Reactions were performed in the presence (+*RT*) or absence (−*RT*) of reverse-transcriptase enzyme. PCR products were digested with a restriction endonuclease to confirm cDNA identity (*cut*). Primers were used to amplify ENaC, uromodulin, γGT, Kir2.3, Kir2.2 and Kir2.1 (see Table 1). In each case, a product was isolated from the whole-cortex sample, but there was no product for γGT, uromodulin, Kir2.1 or Kir2.2 obtained from cortical collecting duct samples. In the *left lane of each panel*, a 100-bp ladder was run and the 500-bp marker is indicated (n = at least 3 separate samples).

tively, were not detected. Neither Kir2.1 nor Kir2.2 was detected in collecting duct samples.

Discussion

The mean capacitance of patches was around 11 pA. Previous studies have measured the capacitance of single rat principal cells at 29 pF (Bubien, 1995) and mouse principal M1 cell capacitance between 8 and 14 pF (Korbmacher et al., 1993; Chalfant, O'Brien & Civan, 1996). The 11 pA capacitance recorded in this study is within the range for M1 cells, suggesting that, as expected for a tight epithelium, current recordings represented only one cell. A similar lack of electrical coupling has been observed in the nasal epithelium of mice (Tarran et al., 1998).

From the current-clamp studies, two types of cells were identified based on their electrophysiological profiles. One cell type showed high Cl^- selectivity, consistent with intercalated cells (Muto et al., 1990). These cells showed a raised profile from the tubule. The second cell type had high K^+ selectivity, consistent with principal cells (Koeppen, Biagi & Giebisch, 1983). These cells showed a flatter morphology within the collecting duct. A similar electrophysiological and morphological profile was recently observed in whole-cell recordings from rat cortical collecting duct (Gray et al., 2005). In addition, a recent single-channel study also reported that K^+ and Cl^- channels in mouse distal tubule and collecting duct are found in different cells (Nissant et al., 2006). The PCR data support a collecting duct phenotype for the tubules used in the study. RNA taken from ducts isolated using the same criteria as in the electrophysiological studies were positive for the collecting duct marker ENaC but negative for γGT and uromodulin, markers of proximal tubules and thick ascending limbs.

Properties of the Total Current

The total current recorded from principal cells had a characteristic profile, with time-dependent inactivation of the currents observed, particularly at positive potentials. This inactivation was associated with an increase in K^+ selectivity as the V_{rev} of steady-state currents was closer to E_K than the V_{rev} of the initial currents. Previous work has demonstrated the presence of a quinidine-sensitive outwardly rectifying conductance in these cells, which has a relatively low K^+ selectivity (Millar et al., 2006). Inactivation of this conductance produces the increase in K^+ selectivity observed at steady state. Given the contamination of the initial K^+ currents by the quinidine-sensitive conductance, the properties of the steady-state currents are a truer reflection of the properties of the K^+-selective currents in the cells. The steady-state currents were highly K^+-selective, with a K^+:Na^+ selectivity ratio of 40. The currents demonstrated inward rectification with a low bath K^+, with the conductance at −100 mV three times greater than the conductance at +100 mV. Strong inward rectification was also observed with high bath K^+, with the conductance at −100 mV five times greater than the conductance at +100 mV. Given the fact that these experiments were carried out in the nominal absence of Mg^{2+}, this suggests that the K^+ currents in the

cells showed a marked Mg^{2+}-independent inward rectification.

Properties of the Ba^{2+}-Sensitive Current

The currents sensitive to 5 mM Ba^{2+} (*I*KBa) were taken as a measure of the magnitude of K^+-selective currents in the cells. *I*KBa was also highly K^+-selective, with a steady-state K^+:Na^+ selectivity ratio of 50. This was similar to the value obtained for the total current, suggesting that *I*KBa dominated the total current. This was also supported by the fact that Ba^{2+} inhibited around 80% of the total current over the negative potential range. *I*KBa demonstrated a characteristic profile, showing strong inward rectification with both low and high bath K^+. With low bath K^+, GKBa at −40 mV was 8.89 ± 1.89 times greater than GKBa at +40 mV (n = 10). With high bath K^+, GKBa at −40 mV was 4.56 ± 1.36 times greater than GKBa at +40 mV (n = 7). This rectification was associated with an apparent inactivation of *I*KBa at positive potentials (Fig. 5). However, there are two possible explanations for this high degree of rectification of *I*KBa. The first explanation is that the block with Ba^{2+} was not maximal at positive potentials and, therefore, the current magnitudes were underestimates. Certainly, the dose-response data clearly show that 5 mM Ba^{2+} is not maximal at potentials more positive than +20 mV. The block by Ba^{2+} was also voltage-dependent. Therefore, under this circumstance, the rectification would be less than described previously. The second possibility is that the inactivation reflects a true rectification. The total current in the absence of Ba^{2+} certainly shows inactivation; however, it is clear from the V_{rev} values that initial currents are less K_+-selective and probably reflect a contribution from the quinidine-sensitive current. Therefore, although a contribution from true rectification cannot be absolutely ruled out, the rectification of *I*KBa is most likely a consequence of voltage-dependent block by Ba^{2+}. In spite of the problem with Ba^{2+} blockade, it is still possible to obtain an estimate of the rectification of *I*KBa with symmetrical K^+. In the first instance, the rectification of the total steady-state current can be examined. The contribution of *I*KBa to the total inward current is high (Fig. 4C), although there is a small contaminating outward conductance, and the total current rectification should therefore provide an estimate of the minimum degree of rectification of the current. The total conductance at −40 mV was 2.36 ± 0.33 times the conductance at +40 mV (n = 14). An estimate of the maximum rectification is provided by *I*KBa. In symmetrical K^+ solutions, the total Ba^{2+}-sensitive conductance at −40 mV was 4.56 ± 1.36 times the conductance at +40 mV (n = 7). The true rectification of the current at +40 mV therefore probably lies between 2.36 and 4.56.

Rectification of *I*KBa was present even when Mg^{2+} was absent from the intracellular solution. Previous work on inwardly rectifying K^+ channels has clearly demonstrated that rectification arises as a consequence of block by intracellular Mg^{2+} and polyamines over positive potential ranges (Fujiwara & Kubo, 2002; Guo & Lu, 2003; Guo et al., 2003). Under the current experimental conditions, both of these were absent, suggesting that an additional mechanism underlies inward rectification of *I*KBa. Other possibilities include Na^+-induced rectification, as has been observed in TASK-2 (Morton et al., 2005). However, in the TASK-2 study, this rectification was only observed initially on achieving the whole-cell configuration and was lost by 1 min. In the current experiments, Na^+ was absent from the pipette solution and no changes in rectification were observed over time, suggesting that it is unlikely that Na^+ could be mediating the rectification observed. Another possibility is block by pipette HEPES. The strongly inward rectifying K^+ channel Kir2.1 has been shown to be sensitive to the presence of HEPES at its intracellular surface (Guo and Lu, 2005). However, 10 mM HEPES, the concentration also used in the current study, did not give any rectification at +40 mV. This contrasts with *I*KBa as rectification was observed at +40 mV in both *I*KBa and the total current under the same experimental conditions. However, this difference could be a consequence of a different source of HEPES as Guo & Lu (2005) found different degrees of rectification with the same concentration of HEPES from different sources.

Kinetics of Block by Ba^{2+}

A previous study on Kir2.1 investigated in some detail the kinetics of inhibition by Ba^{2+} (Shieh et al., 1998). However, such detailed analysis of other Kir2.X channels or native strong inwardly rectifying collecting duct K^+ currents has not been completed. Given the fact that *I*KBa is not attributable to Kir2.1 (see PCR data, Results), a full analysis of the effect of Ba^{2+} was carried out.

There are several pieces of evidence indicating that the inhibition of *I*KBa by Ba^{2+} was voltage-dependent. Firstly, inhibition by 5 mM Ba^{2+} was reduced at potentials more positive than +20 mV. Secondly, the K_d values measured over the potential range −20 to −100 mV decreased with increasing negativity. Thirdly, addition of low Ba^{2+} concentrations gave an increase in inhibition at more negative potentials. This increase in inhibition was associated with a fall in the time constant of inhibition. Fourthly, the association constant (K_{on}) increased with hyperpolarization, suggesting that the rate of Ba^{2+} entry to the pore was greater with more nega-

tive potentials. Taken together these properties indicate enhanced inhibition by Ba^{2+} over the negative potential range. Interestingly, the dissociation constant (K_{off}) also increased with hyperpolarization. This increase in K_{off} is consistent with Ba^{2+} ions dissociating into the pipette solution and was also observed in another inwardly rectifying K^+ channel (Kir2.1) and a Ca^{2+}-activated K^+ channel (Neyton & Miller, 1988; Shieh et al., 1998). Modeling data using the Woodhull equation gave an estimate of the electrical distance of Ba^{2+} block of between 3.7% and 10.2%, suggesting that the Ba^{2+} binding site is located close to the outer surface of the pore.

Comparison to Previously Identified K^+ Channels

*I*KBa represents the mean Ba^{2+}-sensitive current in the principal cells and could therefore be comprised of more than one channel type. Previous studies have identified four Ba^{2+}-sensitive K^+ channels at the molecular level in principal cells from the cortical collecting duct and one in the basolateral membrane of distal nephron, although the specific cell type was not identified. One of these is a Ca^{2+}-activated K^+ channel (Woda et al., 2001). However, this cannot contribute to *I*KBa as the Ca^{2+} in the pipette was at such a level that this channel would be inactive. Another possibility is the apical membrane K^+ channel or basolateral K^+ channels. At the molecular level, the apical K^+ channel is attributable to ROMK (Kir1.1) (Ho et al., 1993; Xu et al., 1997). The basolateral K^+ channel may be attributable to Kir4.1, Kir7.1 or Kir2.3 (Ito et al., 1996; Ookata et al., 2000; Welling, 1997). For Kir2.3, evidence for this comes only from expression studies in MDCK cells (Welling, 1997; Le Maout et al., 1997), although it is known that mRNA for Kir2.3 is found in the whole kidney. In the current study, mRNA was found in whole-cortex tubule samples, suggesting that Kir2.3 is found in cortical nephron segments. In addition, the current study provides direct evidence for the expression of mRNA for Kir2.3 in mouse cortical collecting ducts. RNA from isolated collecting ducts was positive for the collecting duct marker ENaC but negative for markers of proximal tubule and thick ascending limb. The lack of detection of these markers was not a consequence of technical problems as both proximal tubule and thick ascending limb markers were detected in whole-cortex samples. Therefore, it is clear that message for Kir2.3 is found in mouse collecting ducts. The biophysical properties of *I*KBa could also be consistent with the strong inward rectifiers Kir2.1 and Kir2.2. However, mRNA for these channels was not found in collecting duct, although it was detected in whole-cortex samples. A recent study indicates that the dominant conductance in rat principal cells is the basolateral K^+ conductance, although in rat the properties of this conductance do not match those of Kir2.3 (Gray et al., 2005).

Like *I*KBa ROMK is an inward rectifier. However, in contrast to *I*KBa, ROMK demonstrates weak inward rectification. In voltage-clamp experiments using ROMK-expressing oocytes, the inward current was only 1.18 times the outward current (Zhou et al., 1996). This weak inward rectification arises as a consequence of inhibition of outward currents by intracellular Mg^{2+} (Nichols, Ho & Hebert, 1994; Spassova & Lu, 1998). Removal of intracellular Mg^{2+} abolishes the weak rectification observed with ROMK, leading to an ohmic profile in symmetrical K^+ solutions. Such an ohmic profile is observed even when HEPES is present in the pipette. ROMK is also sensitive to block by Ba^{2+}, with a K_d at 0 mV of between 4.7 and 10 mM and an electrical distance of 42% (Zhou et al., 1996; Loffler & Hunter, 1997). Kir7.1, another inward rectifier, demonstrates an unusual *I-V* relationship and has a K_d for block by Ba^{2+} of 670 μM at −100 mV (Döring et al., 1998). Kir4.1, on the other hand, demonstrates moderate inward rectification, requires Mg-ATP to maintain channel activity in excised patches (Takumi et al., 1995) and is likely to form heteromeric channels with Kir5.1 in the mouse distal convoluted tubule (Lourdel et al., 2002). Kir2.3 is a strong inward rectifier that was cloned from a mouse collecting duct cell line (Welling, 1997). In expression studies with low bath K^+, Kir2.3 shows a peak current at −25 mV, with a subsequent decrease in current at more positive potentials. Estimating the rectification of whole-cell Kir2.3 currents in symmetrical K^+ suggests that the current at −40 mV is approximately six times greater than that at +40 mV (Le Maout et al., 1997). Kir2.3 is also sensitive to Ba^{2+}, demonstrating voltage-dependent inhibition, a K_d at 0 mV of 364 μM and an electrical distance of 18% (Welling, 1997).

How do the properties of *I*KBa compare to ROMK, Kir7.1, Kir4.1 and Kir2.3? In the first instance, the experiments detailed here were carried out in the absence of intracellular Mg^{2+}. Under these experimental circumstances, ROMK should give an ohmic profile, even in the presence of HEPES (Nichols et al., 1994; Lu & MacKinnon, 1994). The distal convoluted tubule Kir4.1/5.1 heteromeric channels also lose rectification in the absence of Mg^{2+} (Lourdel et al., 2005). However, *I*KBa demonstrated inward rectification in the absence of Mg^{2+}. The degree of rectification was similar to that observed in Kir2.3, although a direct comparison is complicated by the presence of intracellular Mg^{2+} in the Kir2.3 study. Certainly, the profile of *I*KBa is closer to Kir2.3. The Ba^{2+} sensitivity of *I*KBa is also closer to Kir2.3 than ROMK or Kir7.1. The K_d at 0 mV for block of *I*KBa with Ba^{2+} is 335 μM, while that for Kir2.3 is 364 μM (Welling, 1997). In addition, the electrical distance experienced by the

blocking Ba^{2+} ion is similar, 8% *vs.* 18% for *I*KBa and Kir2.3, respectively. These values are very different from the block of ROMK by Ba^{2+}, with a K_d at 0 mV of 4.7–10 mM and an electrical distance of 42% (Zhou et al., 1996; Loffler & Hunter, 1997). For Kir7.1, the K_d at −100 mV is 670 μM (Döring et al., 1998), while for *I*KBa it is around 20 μM (Fig. 7). The activity for *I*KBa was maintained during experiments in the absence of any pipette ATP. This is in contrast to Kir4.1, which requires the presence of Mg-ATP to maintain channel activity (Takumi et al., 1995), and is further evidence that *I*KBa is not attributable to Kir4.1. Finally, with both *I*KBa and Kir2.3, the potential at which the peak current is observed is similar, −25 mV for Kir2.3 and −20 mV for *I*KBa. Gray et al. (2005) reported an inwardly rectifying K^+ conductance in rat principal cells. This conductance showed weak rectification with high extracellular K^+ but was inhibited by Ba^{2+} in a similar fashion to *I*KBa and Kir2.3 (K_d at 0 mV is 333 μM and the electrical distance is 23%). The molecular nature of this conductance is not known but is unlikely to be Kir2.3 given its poor inward rectification. Finally, two additional K^+ channels have been observed in the distal nephron. The first channel, observed on the basolateral membrane of mouse distal convoluted tubule, shows an ohmic profile in the absence of Mg^{2+} and is thought to be attributable to Kir4.1/5.1 (Lourdel et al., 2002). The second was observed in rat inner medullary collecting duct cells (Escobar et al., 2004). However, it is a voltage-gated channel that acts as a delayed rectifier and probably represents Kv1.3. Given the location and properties of these two channels, it is unlikely that they represent *I*KBa.

In conclusion, the current study demonstrates whole-cell K^+ currents in principal cells from mouse kidney cortical collecting duct. The K^+ conductance shows strong inward rectification, high K^+ selectivity and inhibition by Ba^{2+} in a concentration- and voltage-dependent manner. The properties of the conductance are not consistent with ROMK K^+ channels but are consistent with Kir2.3. Previous work using expression studies has suggested that Kir2.3 forms the dominant basolateral K^+ channel in principal cells. The conductance described here is the first report of a macroscopic K^+ conductance in mouse principal cells that shares the biophysical profile of Kir2.3. The properties and dominant nature of the conductance suggest that it plays an important role in K^+ handling in the principal cells of the cortical collecting duct.

We gratefully acknowledge the financial support of the Biotechnology and Biological Sciences Research Council (BBSRC). I. D. M. is currently at the Faculty of Life Sciences, University of Manchester.

References

Bubien, J.K. 1995. Whole-cell sodium conductance of principal cells freshly isolated from rat cortical collecting duct. *Am. J. Physiol.* **269:**C791–C796

Chalfant, M.L., O'Brien, T.G., Civan, M.M. 1996. Whole-cell and unitary amiloride-sensitive sodium currents in M-l mouse cortical collecting duct cells. *Am. J. Physiol.* **270:**C998–C1010

Döring, F., Derst, C., Wischmeyer, E., Karschin, C., Schneggenburger, R., Daut, J., Karschin, A. 1998. The epithelial inward rectifier channel Kir7.1 displays unusual K^+ permeation properties. *J. Neurosci.* **18:**8625–8636

Doyle, D.A., Cabral, J.M., Pfuetzner, R.A., Kuo, A., Gulbis, J.M., Cohen, S.L., Chait, B.T., MacKinnon, R. 1998. The structure of the potassium channel: Molecular basis of K^+ conduction and selectivity. *Science* **280:**69–77

Escobar, L.I., Martínez-Téllez, J.C., Salas, M., Castilla, S.A., Carrisoza, R., Tapia, D., Vázquez, M., Bargas, J., Bolívar, J.J. 2004. A voltage-gated K^+ current in renal inner medullary collecting duct cells. *Am. J. Physiol.* **286:**965–974

Fujiwara, Y., Kubo, Y. 2002. Ser165 in the second transmembrane region of the Kir2.1 channel determines its susceptibility to blockade by intracellular Mg^{2+}. *J. Gen. Physiol.* **120:**677–692

Gray, D.A., Frindt, G., Zhang, Y.-Y., Palmer, L.G. 2005. Basolateral K^+ conductance in principal cells of rat CCD. *Am. J. Physiol.* **288:**493–504

Guo, D., Lu, K. 2003. Interaction mechanisms between polyamines and IRK1 inward rectifier K^+ channels. *J. Gen. Physiol.* **122:**485–500

Guo, D., Lu, K. 2005. Pore block versus intrinsic gating in the mechanisms of inward rectification in strongly rectifying IRK1 channels. *J. Gen. Physiol.* **116:**561–568

Guo, D., Ramu, Y., Klem, A.M., Lu, K. 2003. Mechanism of rectification in inward-rectifier K^+ channels. *J. Gen. Physiol.* **121:**261–275

Hamill, O.P., Marty, A., Neher, E., Sakmann, B., Sigworth, F.J. 1981. Improved patch clamp techniques for high resolution current recording from cells and cell free membrane patches. *Pfluegers Arch.* **391:**85–100

Ho, K., Nichols, C.G., Lederer, W.J., Lytton, J., Vassilev, P.M., Kanazirska, M.V., Hebert, S.C. 1993. Cloning and expression of an inwardly rectifying ATP-regulated potassium channel. *Nature* **362:**31–38

Holmgren, M., Smith, P.L., Yellen, G. 1997. Trapping of organic blockers by closing of voltage-dependent K^+ channels. Evidence for trap door mechanism of activation gating. J. Gen. Physiol. **109:**527–535

Ito, M., Iananobe, A., Horio, Y., Hibino, H., Isomoto, S., Ito, H., Mori, K., Tonosaki, A., Tomoike, H., Kurachi, Y. 1996. Immunolocalisation of an inwardly rectifying K^+ channel K_{AB}-2 (Kir4.1) in the basolateral membrane of renal distal tubular epithelia. *FEBS Lett.* **388:**11–15

Koeppen, B.M., Biagi, B.A., Giebisch, G. 1983. Intracellular microelectrode characterization of the rabbit cortical collecting duct. *Am. J. Physiol.* **244:**F35–F47

Korbmacher, C., Segal, A.S., Fejes-Toth, G., Giebisch, G., Boulpaep, E.L. 1993. Whole-cell currents in single and confluent M-1 mouse cortical collecting duct cells. *J. Gen. Physiol.* **102:**761–793

Kubo, Y., Baldwin, T.J., Jan, Y.N., Jan, J.Y. 1993. Primary structure and functional expression of a mouse inward rectifier potassium channel. *Nature* **362:**127–133

Le Maout, S., Brejon, M., Olsen, O., Merot, J., Welling, P.A. 1997. Basolateral membrane targeting of a renal-epithelial inwardly rectifying potassium channel from the cortical collecting duct, CCD-IRK3, in MDCK cells. *Proc. Natl. Acad. Sci. USA* **94:**13329–13334

Lesage, F., Guillemare, E., Fink, M., Duprat, F., Lazdunski, M., Romey, G., Barhanin, J. 1996. TWIK-1, a ubiquitous human weakly inward rectifying K^+ channel with a novel structure. *EMBO J.* **15:**1004–1011

Loffler, K., Hunter, M. 1997. Cation permeation and blockade of ROMK1, a cloned renal potassium channel. *Pfluegers Arch.* **434:**151–158

Lourdel, S., Paulais, M., Cluzeaud, F., Bens, M., Tanemoto, M., Kurachi, Y., Vandewalle, A., Teulon, J 2002. An inward rectifier K^+ channel at the basolateral membrane of the mouse distal convoluted tubule: Similarities with Kir4-Kir5.1 heteromeric channels. *J. Physiol.* **538:**391–404

Lu, M., Wang, W.-H. 1998. Reaction of nitric oxide with superoxide inhibits basolateral K^+ channels in the rat CCD. *Am. J. Physiol.* **275:**C309–C316

Lu, Z., MacKinnon, R. 1994. Electrostatic tuning of Mg2 + affinity in an inward-rectifier K^+ channel. *Nature* **371:**243–246

Millar, I.D., Taylor, H.C., Cooper, G.J., Kibble, J.D., Barhanin, J., Robson, L. 2006 Adaptive downregulation of a quinidine-sensitive cation conductance in renal principal cells of TWIK-1 knockout mice. *Pfluegers Arch.* DOI: 10.1007/s00424-006-01070

Morton, M.J., Chipperfield, S., Abohamed, A., Sivaprasadarao, A., Hunter, M. 2005. Na^+-induced inward rectification in the two-pore domain K^+ channel, TASK-2. *Am. J. Physiol.* **288:**F162–F169

Muto, S., Yasoshima, K., Yoshitomi, K., Imai, M., Asano, Y. 1990. Electrophysiological identification of α- and β-intercalated cells and their distribution along the rabbit distal nephron segments. *J. Clin. Invest.* **86:**1829–1839

Neyton, J., Miller, C. 1988. Discrete Ba^{2+} block as a probe of ion occupancy and pore structure in the high conductance Ca^{2+}–activated K^+ channel. *J. Gen. Physiol.* **92:**569–586

Nichols, C.G., Ho, K., Hebert, S. 1994. Mg^{2+}-dependent inward rectification of ROMK1 potassium channels expressed in Xenopus oocytes. *J. Physiol.* **476:**399–409

Nissant, A., Paulais, M., Lachheb, S., Lourdel, S., Teulon, J. 2006. Similar chloride channels in the connecting tubule and cortical collecting duct of the mouse kidney. *Am. J. Physiol.* 290:F1421–F1429

Ookata, K., Tojo, A., Suzuki, Y., Nakamura, N., Kimura, K., Wilcox, C.S., Hirose, S. 2000. Localisation of inward rectifier potassium channel Kir7.1 in the basolateral membrane of distal nephron and collecting duct. *J. Am. Soc. Nephrol.* **11:**1987–1994

Schafer, J.A., Watkins, L., Li, L., Herter, P., Haxelmans, S., Schlatter, E. 1998. A simplified method for isolated of large numbers of defined nephron segments. *Am. J. Physiol.* **273:**F650–F657

Shieh, R.-C., Chang, J.-C., Arreola, J. 1998. Interaction of Ba^{2+} with the pores of the cloned inward rectifier K^+ channels Kir2.1 expressed in Xenopus oocytes. *Biophys. J.* **75:**2313–2322

Spassova, M., Lu, K. 1998. Coupled ion movement underlies rectification in an inward rectifier K^+ channel. *J. Gen. Physiol.* **112:**211–221

Takumi, T., Ishii, T., Horio, Y., Morishige, K.-I., Takahashi, N., Yamada, M., Yamashita, T., Kiyama, H., Sohmiya, K., Nakanishi, S., Kurachi, Y. 1995. A novel ATP-dependent inward rectifier potassium channel expressed predominantly in glial cells. *J. Biol. Chem.* **270:**16339–16346

Tarran, R., Gray, M.A., Evans, M.J., Colledge, W.H., Ratcliff, R., Argent, B.E 1998. Basal chloride currents in murine airway epithelial cells: Modulation by CFTR. *Am. J. Physiol.* **274:**C904–C913

Wang, W.-H. 1995. Regulation of the hyperpolarization-activated K^+ channel in the lateral membrane of the cortical collecting duct. *J. Gen. Physiol.* **106:**25–43

Welling, P.A. 1997. Primary structure and functional expression of a cortical collecting duct Kir channel. *Am. J. Physiol.* **273:**825–836

Woda, C.B., Bragin, A., Kleyman, T.R., Satlin, L.M. 2001. Flow-dependent K^+ secretion in the cortical collecting duct is mediated by a maxi-K channel. *Am. J. Physiol.* **49:**F786–F793

Xu, J.Z., Hall, A.E., Peterson, L.N., Bienkowski, M.J., Eessalu, T.E., Hebert, S.C. 1997. Localization of the ROMK protein on apical membranes of rat kidney nephron segments. *Am. J. Physiol.* **273:**F739–F748

Zhou, H., Chepliko, S., Schutt, W., Choe, H., Palmer, L.G., Sackin, H. 1996. Mutations in the pore region of ROMK enhance Ba^{2+} block. *Am. J. Physiol.* **271:**C1949–C1956